Ceramics International 47 (2021) 7728–7737

Contents lists available at ScienceDirect

Ceramics International

journal homepage: www.elsevier.com/locate/ceramint

Improvement of gas sensing property for two-dimensional $Ti_3C_2T_x$ treated with oxygen plasma by microwave energy excitation

Ming Hou [a,c,e], Shenghui Guo [a,c], Li Yang [a,b,c,*], Jiyun Gao [c,d], Tu Hu [c], Xinwei Wang [b,**], Yongxiang Li [e]

[a]. State Key Laboratory of Complex Nonferrous Metal Resources Clean Utilization, Kunming University of Science and Technology, Kunming 650093, China
[b]. Department of Mechanical Engineering, Iowa State University, Ames 50011, USA
[c]. Faculty of Metallurgical and Energy Engineering, Kunming University of Science and Technology, Kunming 650093, China
[d]. School of Chemistry and Environment, Yunnan Minzu University, Kunming 650093, China
[e]. School of Electronic and Telecommunication Engineering, RMIT University, Melbourne VIC 3000, Australia

ARTICLE INFO

Keywords:
Two-dimensional materials
MXene $Ti_3C_2T_x$
Gas sensing property
Volatile organic compounds
Oxygen microwave plasma treatment
Functional group regulation

ABSTRACT

Two-dimensional layered $Ti_3C_2T_x$ MXene was prepared through hydrothermal etching method with LiF and hydrochloric (HCl) acid. $Ti_3C_2T_x$ was further treated with oxygen plasma activated by microwave energy to obtain the activated $Ti_3C_2T_x$ at different temperatures ranging from 350 °C to 550 °C. The gas-sensing properties of raw $Ti_3C_2T_x$ and $Ti_3C_2T_x$ activated with oxygen microwave plasma were tested toward different volatile organic compounds gases. The results indicated that $Ti_3C_2T_x$ activated at 500 °C exhibited excellent gas-sensing properties at room temperature (25 °C) to 100 ppm ethanol with a value of 22.47, which is attributed to the enhancement of the amount of oxygen functional groups and defects on the MXene $Ti_3C_2T_x$ film, and in turn to lead to more oxygen molecules adsorption and desorption reaction in the active defect sites. The enhancement of ethanol-sensing performance demonstrated that the activated $Ti_3C_2T_x$ possess great potential in gas sensing.

1. Introduction

With the development of industry and socio-economy, more and more volatile organic compounds (VOCs) are being produced; however, they are toxic air pollutants, which can impact on human health directly [1–7]. In the field of petroleum processing, a large amount of ethanol or methanol gas leakage happens. This will expand and cause casualties and property damages [8,9]. Exposure to benzene could give rise to polycythemia and aplastic anemia [10]. Prolonged inhalation of toluene could cause paralysis and dysfunction in human body [11]. Hexane vapors could give rise to irritation of throats and eyes [12]. Therefore, the preparation of a highly sensitive, selective and stable sensor towards VOCs which can act as an alarm for VOCs leakage has become a necessary work and an important goal in applications for industrial development.

Currently, metal oxide semiconductor (MOS), which has high sensitivity, low cost and simplicity in function [13–15], is widely studied as the core material for VOCs sensors. Feng and his co-workers prepared a novel Au@ZnO sensor with exchange method. The sensor based on Au@ZnO exhibited fortified sensitivity at 400 °C to different kinds of VOCs compared with raw ZnO [16]. In spite of MOS showing superior sensitivity, all the operating temperatures exceed 100 °C, and even reach to 400 °C. High operating temperatures limit the application of MOS sensors in wearable sensing device area. Therefore, it is urgent to explore a novel and suitable material for more superior sensing ability at lower temperature.

Nowadays, two-dimensional (2D) materials which feature promising properties such as carbon nanomaterial, black phosphorene and metal organic framework have attracted more and more attention as candidate materials for energy storage and sensors [17–20]. However, they are subjected to low stability or poor gas-sensing properties in the field of gas sensing, which seriously limit the applications. In all 2D materials, MXene, a booming 2D material family which consists of transition metal carbides, nitrides and carbonitrides, has been extensively studied and it exhibits unique excellent performance due to its metal semiconductor properties and its plentiful surface functional group structure [21–23].

* Corresponding author. State Key Laboratory of Complex Nonferrous Metal Resources Clean Utilization, Kunming University of Science and Technology, Kunming 650093, China.
** Corresponding author.
E-mail addresses: yanglikmust@163.com (L. Yang), xwang3@iastate.edu (X. Wang).

https://doi.org/10.1016/j.ceramint.2020.11.117
Received 30 June 2020; Received in revised form 8 November 2020; Accepted 15 November 2020
Available online 19 November 2020

$Ti_3C_2T_x$ represents a typical MXene, and it is synthesized by etching the intermediate layer from Ti_3AlC_2 MAX phase in aqueous hydrofluoric (HF) acid solutions or mixture of hydrochloric (HCl) acid and lithium fluoride (LiF). After the etching treatment, hydrophilic $Ti_3C_2T_x$ nano flakes can be produced with abundant different functional groups, where T_x represents the surface functional groups, such as –O, –OH, or –F. $Ti_3C_2T_x$ is an organ-like structure with high specific surface area, adjustable nanometer-layer thickness and high conductivity [24]. Therefore, it shows great potential for the application of gas-sensing materials [25]. Kim and his co-authors prepared the gas sensors based on $Ti_3C_2T_x$ and the gas sensors show excellent sensing performance with high signal-to-noise-ratio. Meanwhile, the sensors based on $Ti_3C_2T_x$ exhibited a very low limit of detection of 50–100 ppb for VOC gases at room temperature [26]. Lee et al. also put 2D titanium carbide to the fabrication of wearable gas sensors. The limit of detection of acetone gas was theoretically calculated to be about 9.27 ppm, presenting better performance compared to other 2D material-based sensors [27]. However, the low response value limits its application in the field of sensors. It is worth noting that the modification of terminal groups on the surface of $Ti_3C_2T_x$ can effectively change the sensing properties [28]. Thus, it is important and necessary to orient the functional groups of $Ti_3C_2T_x$ to improve its oxygen affinity.

Microwave plasma has the characteristics of high plasma density and high activity of ionized materials. It is a promising and novel method for CVD synthesis and surface modification of materials. Vlasov and his co-authors prepared ultranano-crystalline diamond film with MPCVD method in Ar-rich atmosphere [29]. Wu et al. fabricated hard and ultra-water-repellent silicon oxide films by combining MPCVD and chemical method. And the films possess high optical transparency [30]. Guo and his co-authors prepared diamond films with high binding strength by using MPCVD process [31]. Raymundo and his co-workers modified the surface of graphene nanoparticles by using ethylene plasma. The compatibility with high-density polyethylene of samples was effectively improved [32]. Unfortunately, to our knowledge, there are no reports on the use of such excellent treatment technology to modify $Ti_3C_2T_x$.

In this work, room temperature ethanol sensors were exploited and prepared based on $Ti_3C_2T_x$ sensing materials. The improved ethanol gas-sensing properties for $Ti_3C_2T_x$ sensors were enforced by MPCVD activation treatment. Under oxide microwave plasma irradiation, there will be many defects generated on the $Ti_3C_2T_x$ plate and large amounts of oxygen functional groups will be produced around $Ti_3C_2T_x$, which enhance the number of oxygen adsorption sites on the film. In addition, the effect of activating temperature on sensing properties and the potential sensing mechanism were studied and discussed. The enhanced sensing properties for the activated $Ti_3C_2T_x$ exhibit excellent application potential in gas sensing.

2. Materials and methods

2.1. Methods of sample preparation

Synthesis of $Ti_3C_2T_x$ MXene: $Ti_3C_2T_x$ was prepared with etching interlayer process according to the previous report [33] and the illustration is shown in Fig. 1(a). Here, Ti_3AlC_2 powders were gradually added into etchant solution and stirred for 24 h at 60 °C. The etchant solution is composed of 1.6 g LiF, 15 mL of hydrochloric acid (37 wt %) and 5 mL of deionized water [34]. After etching treatment, deionized water was used to wash and centrifuge the suspension until the pH of the mixture solution shows litmusless. Then the as-product was put in oven to dry for 12 h at 80 °C. Ultimately, the $Ti_3C_2T_x$ powder with lamellar structure were collected and stored to further use.

Synthesis of activated $Ti_3C_2T_x$ MXene and the fabrication of gas sensor: The synthesis of activated $Ti_3C_2T_x$ MXene was completed in MPCVD reactor. And $Ti_3C_2T_x$ MXene gas sensor was prepared by using dropping method. First, $Ti_3C_2T_x$ was dispersed in ethanol solvent and ultrasonic for 20 min. And $Ti_3C_2T_x$ was dropped on an Al_2O_3 ceramic substrate with interdigitated Pt electrodes and dried in an oven at 70 °C for 12 h to remove moisture. Then the ceramic substrate with $Ti_3C_2T_x$ was put into MPCVD reactor to achieve plasma activation. The illustration is shown in Fig. 1 (b). Under vacuum condition, when the pressure is 0.1 Pa, oxygen is pumped in the reactor chamber. When the pressure increased to 2 KPa, microwave was turned on and uniform plasma can be obtained by adjusting the sample platform. The activation temperature is related to the microwave power and it was checked with infrared temperature measurement. And the ceramic substrate was activated at the target temperature of 350 °C, 400 °C, 450 °C, 500 °C, and 550 °C for 60 min. The ceramic substrate was surrounded by the high energy and density plasma at the whole activation process.

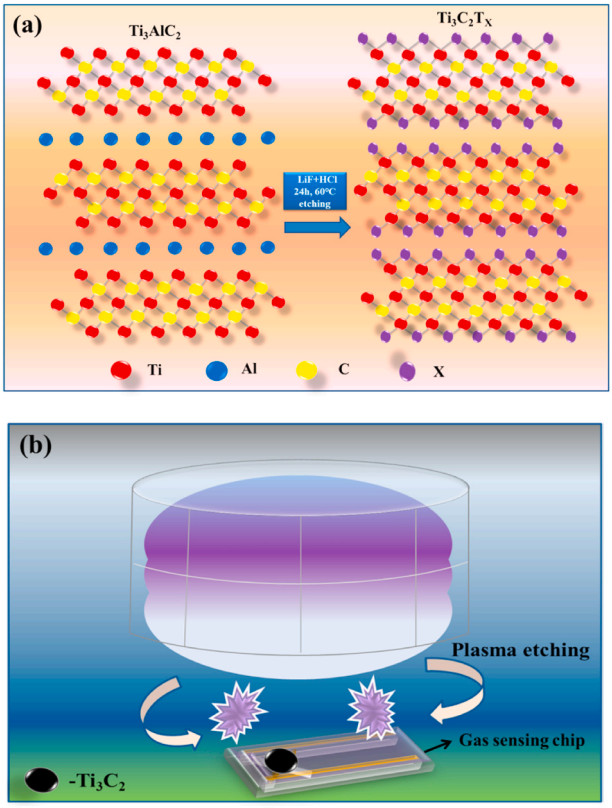

Fig. 1. Schematic illustration of (a) the production of $Ti_3C_2T_x$, and (b) the oxygen plasma treatment process.

2.2. Samples characterization

A field emission scanning electron microscope (FESEM JSM-7100 F, JEOL) was used to check and analyze the microstructure of the $Ti_3C_2T_x$ activated at different temperatures. The crystal phase of samples was studied by applying X-ray diffraction (XRD, Rigaku D/max-2500) using Cu Kα radiation (λ = 1.5418 Å) in the 2θ range from 5° to 70°. X-ray photoelectron spectra (XPS) were recorded using Thermo ESCALAB 250Xi. Raman spectroscopy was recorded to study the molecular structure on a confocal laser micro-Raman spectrometer. The surface area measurements were performed via N_2 adsorption/desorption at −196 °C and calculated by the Brunauer Emmett and Teller (BET) analysis method in the relative pressure range P/P0 = 0.05–0.35. Total pore volumes of the samples were calculated at a relative pressure of P/P0 = 0.99.

2.3. Measurement of gas sensing device

Gas sensing was completed in a four channel gas sensing

measurement device (SD101 , Huachuang Ruike Science and Technology Wuhan Co. Ltd). The electrode chip was fabricated on the basis of an alumina substrate (6*30 mm). The platinum sizing agent was printed on the alumina matrix by using screen printing. Then these alumina matrixes were dried at 70 °C for 40 min and calcined at 350 °C and 850 °C for 20 min. As shown in Fig. 2, the whole platinum electrode was consisted of heating electrode and measuring electrode. The gap between the gear shaping electrodes was 0.42 mm. As displayed in Fig. 2, the $Ti_3C_2T_x$ pastes sensing materials were printed on the alumina matrix by using screen printing method. The thickness of $Ti_3C_2T_x$ films were 5–10 μm, which is achieved by using the screen printing equipment. Then the samples were put in an oven to remove the organic solvent at 70 °C for 40 min. At last, the as-products were annealed at 400 °C for 2 h under argon atmosphere to enhance the mechanical bond of particles in the films.

The gas sensing test sketchy process is as following. First, the test chip is placed in a closed chamber filled with air. Then, when the resistance shows a stable baseline, the sensor was exposed to the target gas for testing at different work temperatures and different gas concentration. This work investigated the gas-sensing properties of $Ti_3C_2T_x$ MXene at room temperature (25 °C), 250 °C, 275 °C, 300 °C, 325 °C, 350 °C, 375 °C and 400 °C. At least 3 samples were tested for each type of sensors and the average values are calculated. The gas response can be evaluated by the following formula:

$$S = \frac{\Delta R}{R_a} \times 100\% \quad , \tag{1}$$

where ΔR represents the difference between the resistance under air and the one under target gas. R_a is the resistance under air.

3. Results and discussion

Microscopic structures of the $Ti_3C_2T_x$ treated with oxygen plasma at different temperatures were checked with FESEM and the results were displayed in Fig. 3. Obviously, the $Ti_3C_2T_x$ obtained by fluoride salt etching show lamellar and organ-like structures. The interlayer spacing of the plasma-activated Ti_3C_2 is significantly higher than that of the non-plasma-activated raw $Ti_3C_2T_x$, which indicates that plasma can promote to open the sheets. With the increase of plasma activating temperature, the opening degree of the samples sheets show an increasing tendency and the structure is more uniform. The samples activated at 500 °C show the most uniform and dense morphology and the distance between the layers is the largest. At the moment, dimples appeared inside the samples sheets which significantly increase the specific surface area of the samples. The specific surface areas of samples activated at different temperature were tested and the results were shown in Table 1. The specific surface area of the sample treated at 500 °C show the highest, which means it can provide more oxygen adsorption sites. Activating temperature continues to increase, fracture of the sample sheet happened and there were debris on the sample surface.

Raman spectra of raw $Ti_3C_2T_x$ and $Ti_3C_2T_x$ treated with oxygen plasma at different temperatures were shown in Fig. 4 (a). There are three characteristic peaks at 399 cm^{-1}, 528 cm^{-1} and 630 cm^{-1}, which represent the $E_{g(1)}$, $B_{1g(1)}$, A_{1g}, and $E_{g(3)}$ vibrational modes of TiO_2, respectively in the spectra of the samples activated with oxygen microwave plasma [34]. This is because the $Ti_3C_2T_x$ was partially oxidized under oxygen plasma activating to generate TiO_2. D peak and G peak were also observed in all spectra and the ratio of I_D/I_G was calculated. It is worth mentioning that the ratio of I_D/I_G represents the chaos and defects of carbon materials. As shown in Fig. 4 (a), the ratio of I_D/I_G of raw $Ti_3C_2T_x$ is 0.85, which indicates that raw $Ti_3C_2T_x$ is in high order. The ratios of samples activated with oxygen plasma are larger than those of raw materials and the ratio of the sample activated at 500 °C is the largest. It is worth mentioning that there are also diffract spectra for $Ti_3C_2T_x$ in the samples activated by oxygen plasma, which proves that $Ti_3C_2T_x$ is not completely transformed into TiO_2, as shown in Fig. 4 (b). The above results proved that defects can be obtained in the $Ti_3C_2T_x$ by using oxygen microwave plasma process. XRD spectra of raw $Ti_3C_2T_x$ and $Ti_3C_2T_x$ activated with oxygen plasma at different temperatures were also studied and the results were displayed in Fig. 5. During the test, the $Ti_3C_2T_x$ samples were dropped on the Al_2O_3 ceramic sheets, so the phase of Al_2O_3 can be found in the test result. Obviously, $Ti_3C_2T_x$ can be prepared by the process of etching the MAX intermediate layer Al with lithium fluoride and HCl. Compared with raw $Ti_3C_2T_x$, there is a new phase of TiO_2 generated on the $Ti_3C_2T_x$ activated with oxygen microwave plasma and the content of TiO_2 is calculated with RIR method based on MDI Jade mode and the formula is shown as following:

$$W_X = \frac{I_X}{K_A^X \sum_{i=A}^{N} \frac{I_i}{K_A^i}} \tag{2}$$

Where W_X is mass content of X phase, I_X is the integral strength of the phase X, K_A^X is the K value of X with A as the internal standard, N is the quantity of phases in samples, I_i is the integral strength of the phase No. i, K_A^i represents to the K value of No. I phase with A as the internal standard.

After calculating, the content of TiO_2 is less than 5%, which means that oxygen microwave plasma will not destroy the original phase structure of $Ti_3C_2T_x$.

Elemental composition and chemical state of raw $Ti_3C_2T_x$ and $Ti_3C_2T_x$ treated with oxygen plasma at different temperatures were checked by using XPS spectra. Fig. 6 proves the existence of Ti, F, O and C elements in raw $Ti_3C_2T_x$ and the $Ti_3C_2T_x$ treated with oxygen plasma at different temperatures. The C 1s spectra show three types of carbon atoms: C-O, C-C and C-Ti-T_x. And the spectra of all the $Ti_3C_2T_x$ activated at different conditions do not show much difference. The proportion –F functional groups of raw $Ti_3C_2T_x$ and $Ti_3C_2T_x$ treated with oxygen microwave plasma at different temperatures can be represented indirectly with the intensity of Ti-F bond peak. As shown in Fig. 6, the Ti-F bond intensity in the peaks of the $Ti_3C_2T_x$ activated with oxygen microwave plasma had an obvious weakening, which means that oxygen microwave plasma can facilitate the removal of –F functional group. When the sample is activated with oxygen plasma, high active oxygen is chemically adsorbed on the surface, competing with F on the surface termination site and F is gradually replaced by O adsorbed on the material surface. With the activating temperature increasing, parts of the adsorbed oxygen atoms are further transformed to form lattice oxygen of TiO_2. The Ti 2p XPS spectra of $Ti_3C_2T_x$ activated with oxygen plasma at different temperatures and raw $Ti_3C_2T_x$ were fitted to 4 different peaks, which represent C-Ti-O_xF_x, TiO_2, C-Ti-O_x and C-Ti-F_x.

It is worth mentioning that the ability of sensitive materials to adsorb and ionize oxygen is critical to the performance of a gas sensor [35–37]. The O 1s spectra of raw $Ti_3C_2T_x$ and $Ti_3C_2T_x$ activated with oxygen plasma at different temperatures were deconvoluted. As shown in Fig. 6, two types of peaks correspond to different oxygen that is adsorbed on the grain surface. O_l refers to lattice oxygen and O_c represents chemisorption and dissociation of oxygen ions [38]. The central peak positions

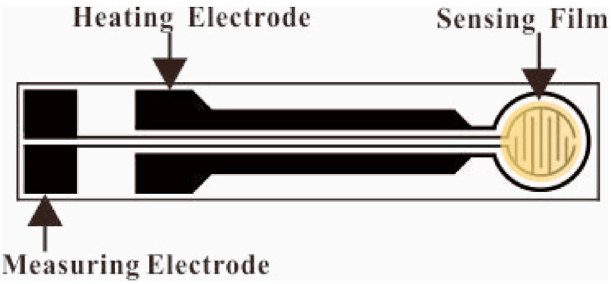

Fig. 2. The schematic diagram of test chip including platinum electrode and sensing material film.

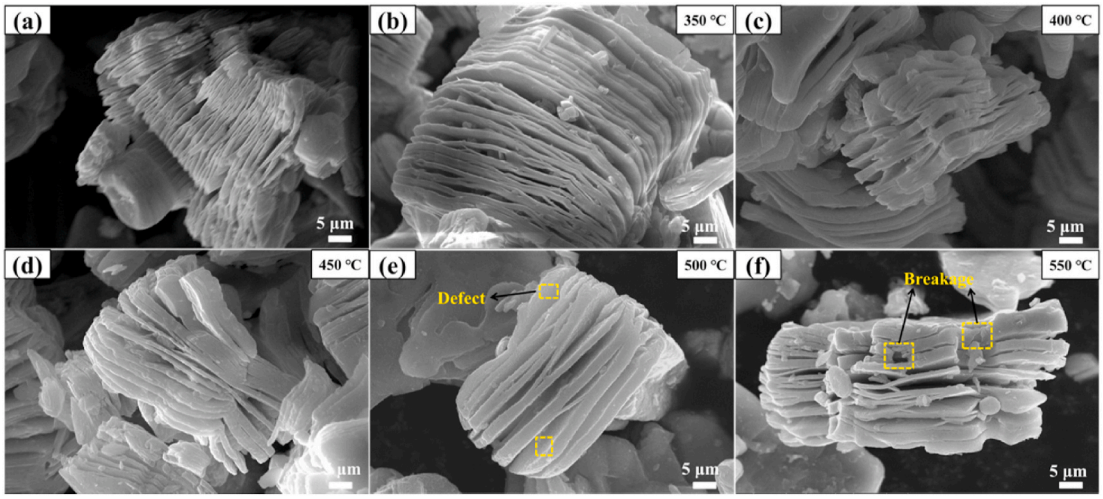

Fig. 3. SEM images of microstructure of $Ti_3C_2T_x$ activated with oxygen plasma at different temperatures.

Table 1
The specific surface areas of $Ti_3C_2T_x$ activated with oxygen plasma at different temperatures.

Temperature (°C)	0	350	400	450	500	550
Specific surface areas (m^2/g)	23.71	47.58	55.60	59.42	63.66	43.19

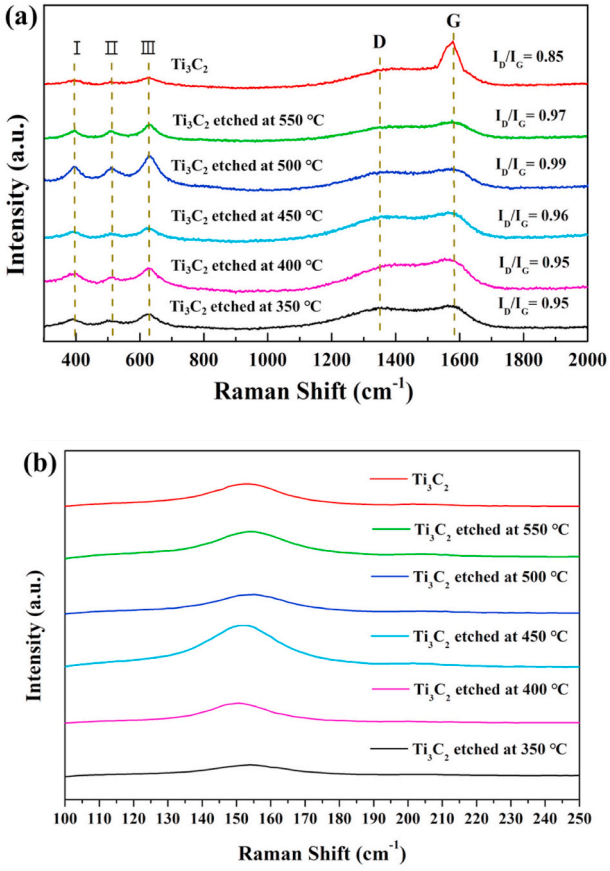

Fig. 4. (a) Raman spectra of raw $Ti_3C_2T_x$ and $Ti_3C_2T_x$ activated with oxygen plasma at different temperatures; (b) Raman spectra of samples in the range of 100–250 cm^{-1}..

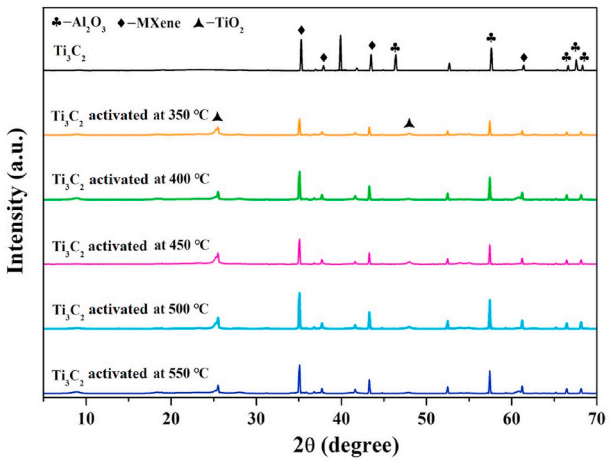

Fig. 5. XRD spectra of raw $Ti_3C_2T_x$ and $Ti_3C_2T_x$ activated with oxygen plasma at different temperatures.

and content percentages of two oxygen peaks of raw $Ti_3C_2T_x$ and $Ti_3C_2T_x$ activated with oxygen plasma at different temperatures are calculated and listed in Table 2. According to Table 2, the O_I values of the $Ti_3C_2T_x$ activated with oxygen microwave plasma become larger than that of raw $Ti_3C_2T_x$ and the samples activated at 550 °C shows the most obvious variation. It means that the part of oxygen adsorbed on the surface of materials is translated into lattice oxygen. The analysis correlates well with that of XRD analysis. It is worth mentioning that although part of the adsorbed oxygen is converted into lattice oxygen, since oxygen replaces fluorine, a large amount of adsorbed oxygen still exists on the material surface, which is beneficial to make the samples to provide more oxygen adsorption sites, leading to greater resistance change. Based on the above analysis, it is reasonable to believe that the oxygen microwave plasma activating method can improve the gas-sensing properties of the samples.

In order to investigate the effect of oxygen microwave plasma activation on the resistance of $Ti_3C_2T_x$, the resistances of $Ti_3C_2T_x$ activated at different temperature were checked and the results were shown in Fig. 7. After activating with oxygen plasma, the resistance of $Ti_3C_2T_x$ increases from kiloohm level to megohm level, which indicates the conductivity of $Ti_3C_2T_x$ gradually transforms from conductor into semiconductor. The conductivity transition behavior is relative to the increment of oxygen functional groups on the surface of $Ti_3C_2T_x$.

To further demonstrate that oxygen microwave plasma activation is

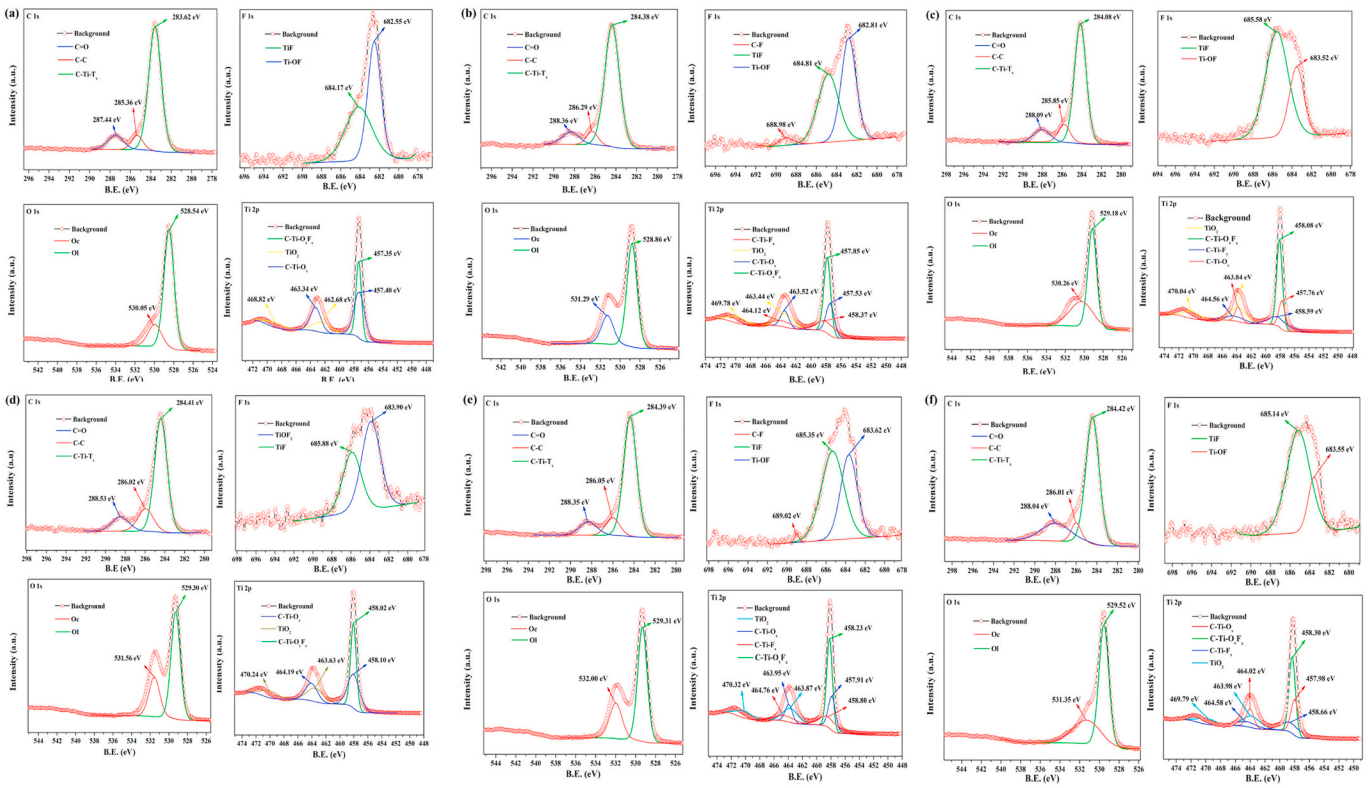

Fig. 6. XPS spectra of $Ti_3C_2T_x$ treated with oxygen plasma at 350 °C, 400 °C, 450 °C, 500 °C and 550 °C, respectively (a, b, c, d and e) and raw $Ti_3C_2T_x$ (f).

Table 2
Fitting results of O1s XPS spectra of raw $Ti_3C_2T_x$ and the $Ti_3C_2T_x$ activated at different temperature.

Materials	Oxygen species	Binding energy (eV)	Relative percentage (%)
Raw $Ti_3C_2T_x$	O_L (Ti-O)	529.52	40.52
	O_C (Chemisorbed)	531.35	59.48
$Ti_3C_2T_x$ activated at 350 °C	O_L (Ti-O)	528.54	49.88
	O_C (Chemisorbed)	530.99	50.12
$Ti_3C_2T_x$ activated at 400 °C	O_L (Ti-O)	528.86	51.38
	O_C (Chemisorbed)	531.29	48.62
$Ti_3C_2T_x$ activated at 450 °C	O_L (Ti-O)	529.18	55.73
	O_C (Chemisorbed)	531.50	44.27
$Ti_3C_2T_x$ activated at 500 °C	O_L (Ti-O)	529.30	62.98
	O_C (Chemisorbed)	531.56	37.02
$Ti_3C_2T_x$ activated at 550 °C	O_L (Ti-O)	529.31	75.74
	O_C (Chemisorbed)	532.00	24.26

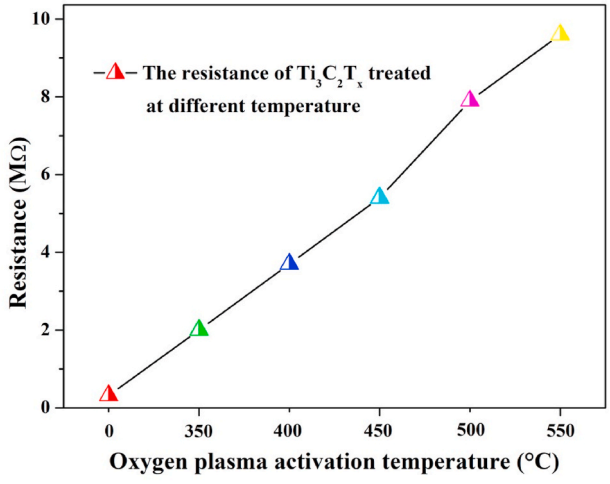

Fig. 7. The air resistance R_a of $Ti_3C_2T_x$ samples treated at different oxygen microwave plasma activation temperature.

an effective method to increase the gas-sensing properties of gas sensor based on MXene, the gas gas-sensing properties of the raw $Ti_3C_2T_x$ and the $Ti_3C_2T_x$ activated at different temperatures with oxygen microwave plasma were studied. To our knowledge, test temperature is the primary factor to affect the sensitive performance of gas-sensitive materials [39–42]. Thus, the gas response of the raw $Ti_3C_2T_x$ and $Ti_3C_2T_x$ activated at different temperatures with oxygen microwave plasma toward 100 ppm ethanol were checked at different testing temperatures from 250 °C to 400 °C to investigate the optimal activating temperature and the effect of testing temperature on gas response. As shown as Fig. 8, as the testing temperature enhance, the response of all the sensors show increasing tendency between 250 °C and 325 °C, and reach a maximum at 325 °C and then show decreasing tendency. Among all the sensors, the sensor based on the $Ti_3C_2T_x$ activated at 500 °C show the highest response to 100 ppm ethanol, with the value of 69, which is 34.7% higher than the response of sensor based on raw $Ti_3C_2T_x$. This result can be explained as below. The oxygen microwave plasma activating method can increase the amount of oxygen functional groups and the defects of the samples, thereby providing more adsorption sites for the oxygen and the increasing of the gas-sensing performance.

The response values of the $Ti_3C_2T_x$ treated with different conditions being exposed to ethanol with different concentrations ranging from 30 to 800 ppm at the best checking temperature is reported in Fig. 9. It can be found that with the increase of gas concentration, all the responses of sensors based on $Ti_3C_2T_x$ treated with different conditions show

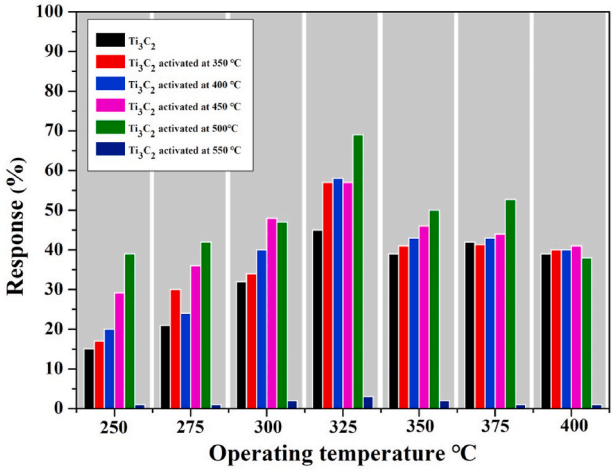

Fig. 8. Gas response of the $Ti_3C_2T_x$ and $Ti_3C_2T_x$ treated with oxygen plasma toward 100 ppm ethanol at different operating temperature.

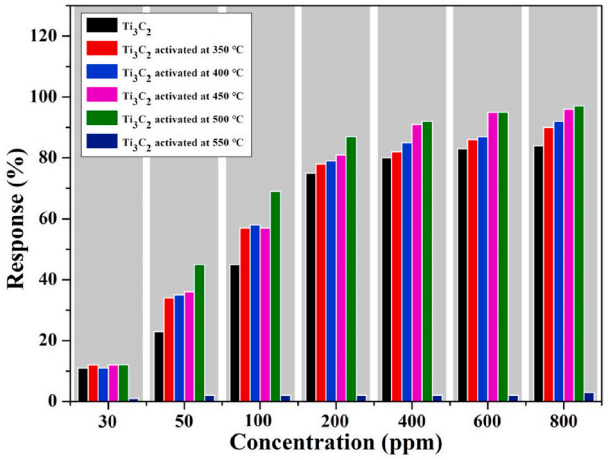

Fig. 9. Gas response of the raw $Ti_3C_2T_x$ and $Ti_3C_2T_x$ treated with oxygen plasma to ethanol at different concentrations at 325 °C.

increasing trends. The response of sensors based on raw $Ti_3C_2T_x$ is 10 for 30 ppm and the response of sensor based on the $Ti_3C_2T_x$ activated at 500 °C is 12 for 30 ppm. Furthermore, the response of the $Ti_3C_2T_x$ activated at 500 °C is the highest among all the sensors at all gas concentration.

Excellent selectivity is one of the important and necessary properties for gas-sensitive materials. Thus, the response of sensors based on $Ti_3C_2T_x$ activated at different conditions upon exposure to different VOCs gases toward 100 ppm at 325 °C were checked and is displayed in Fig. 10. **All sensors show good selectivity and the sensor based on the $Ti_3C_2T_x$ activated at 500 °C shows more obvious in selectivity performance. It could be concluded that activating with oxygen microwave plasma, especially at 500 °C, had a great improvement on sensing properties.**

According to the above analysis of gas sensing properties of the $Ti_3C_2T_x$ treated at different conditions, the $Ti_3C_2T_x$ activated at 500 °C shows excellent performance. It is worth noting that low testing temperature and low gas detection concentration can facilitate the application of samples in gas sensors. Thus, the gas sensing performance of devices based on $Ti_3C_2T_x$ activated at 500 °C was also studied at room temperature and the results were shown in Fig. 11. The response comparisons of the raw $Ti_3C_2T_x$ and $Ti_3C_2T_x$ activated with oxygen plasma to ethanol at room temperature at different concentrations were displayed in Fig. 11 **(a)**. And the response-recovery curve of $Ti_3C_2T_x$ activated

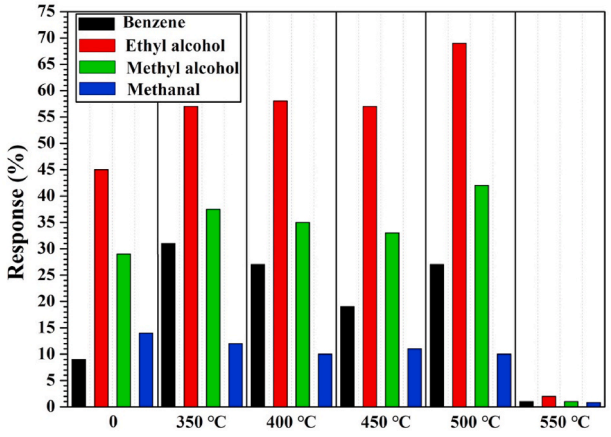

Fig. 10. Gas response of the raw $Ti_3C_2T_x$ and $Ti_3C_2T_x$ treated with oxygen plasma at 350 °C, 400 °C, 450 °C, 500 °C and 550 °C to different 100 ppm target gases at 325 °C.

with oxygen plasma to 10–800 ppm ethanol at room temperature was also shown in Fig. 11 (b). The gas response of $Ti_3C_2T_x$ and activated $Ti_3C_2T_x$ shows enhancing tendency as ethanol concentration increased. The response with the value of 22.47 of the activated $Ti_3C_2T_x$ to ethanol with the concentration of 100 ppm was nearly higher than twice that of the raw $Ti_3C_2T_x$ at room temperature and is also higher than that reported in other literatures [26,43]. For example, the most sensitive VOCs sensor based on MXene fabricated by Hee-Tae Jung displayed 1.75 responses to 100 ppm ethanol, whereas our sensor's response value to the same concentration of ethanol gas under the same conditions is nearly 20 times than theirs [44]. The comparison of the gas-sensing properties toward ethanol among this work and previous works are shown in Table 3. Although metal oxides have higher gas-sensitive responses, they require higher test temperatures. The most significant advantage of the sensors based on $Ti_3C_2T_x$ activated with oxygen microwave plasma is the performance of highly sensing measurement at room temperature, which is impossible for the sensors based on metal oxides. The comparison confirmed that the oxygen microwave plasma activating method has a great advantage in the application of VOCs sensing. Fig. 11 (c) shows the dynamic response-recovery curve of the $Ti_3C_2T_x$ activated with oxygen plasma to ethanol at 100 ppm. It can be seen that the sample displayed the characteristics of an n-type semiconductor and it is consistent with previous reports [43,44]. What is more, it proves that the $Ti_3C_2T_x$ activated with oxygen plasma possess comparatively good repeatability to ethanol with the concentration of 100 ppm during four cycles. The activated $Ti_3C_2T_x$ also displays an excellent selective performance shown in Fig. 11 (d) and the dynamic response-recovery curve of the $Ti_3C_2T_x$ activated with oxygen plasma to different gases at 100 ppm was displayed in Fig. 11 (e), which indicates that the samples possess high anti-interference ability against different gases and high stability in the environment. As far as we know, long-term good stability can insure the accuracy of sensor. Thus, long term stability experiment of the $Ti_3C_2T_x$ activated at 500 °C toward 100 ppm ethanol at room temperature was conducted over 10 days, as shown in Fig. 11 (f). The response values of sensor keep fluctuating up and down at 22.47, which indicate that a smart $Ti_3C_2T_x$ ethanol sensor with excellent stability, high selectivity and superior gas response can be obtained by using oxygen microwave plasma activating method.

Generally, the sensing mechanism of $Ti_3C_2T_x$ for VOCs can be well explained by the resistance change of materials which depends on the capacity of adsorbing oxygen on the material surface. According to the analysis of gas-sensing properties of the samples, the characteristic of the activated $Ti_3C_2T_x$ n-type semiconductor can be obtained. As shown as Fig. 12 (a), when the sample is exposed in air, oxygen molecules will be adsorbed on the sample surface, which will take electrons from the

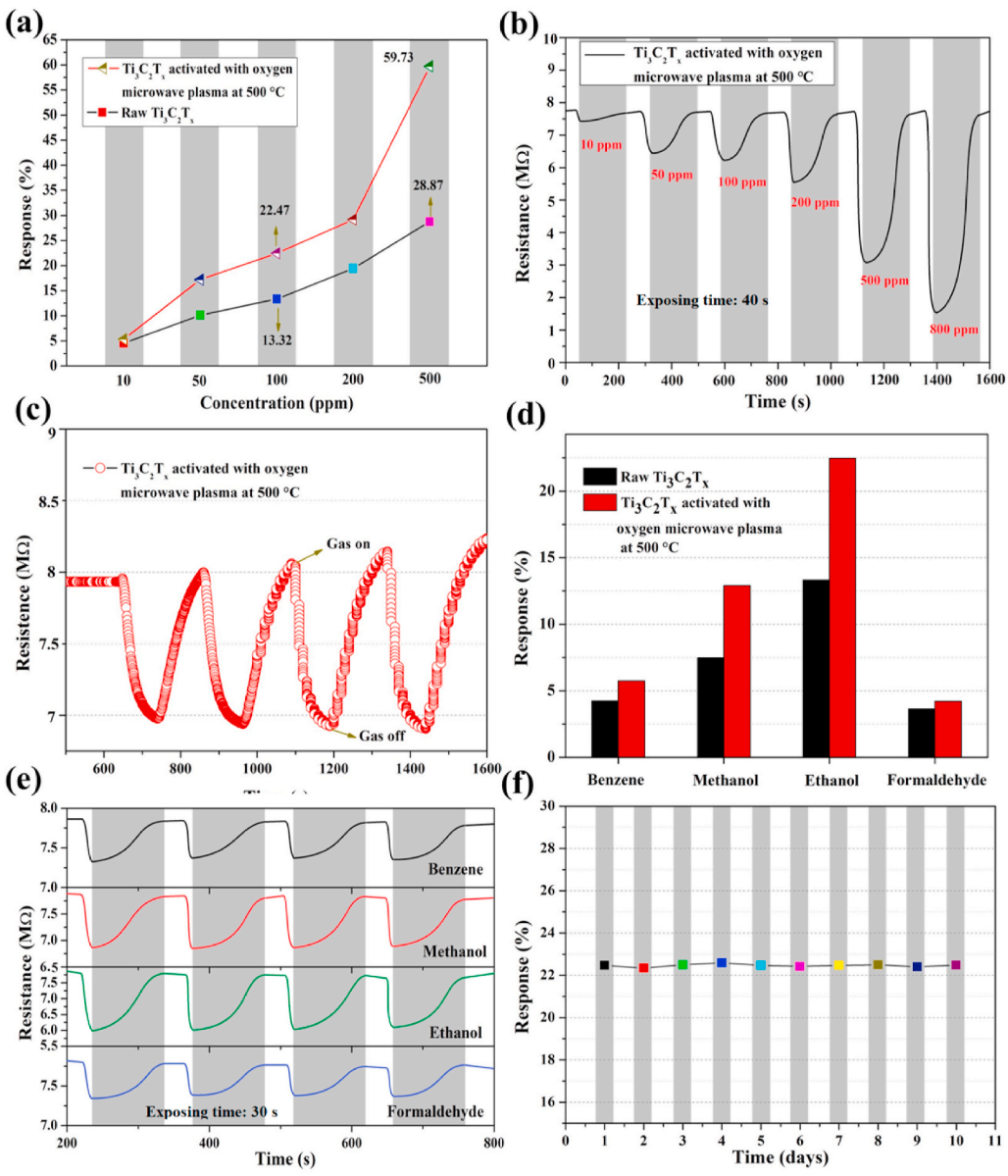

Fig. 11. (a) Gas response of the raw $Ti_3C_2T_x$ and $Ti_3C_2T_x$ activated with oxygen plasma to ethanol at different concentration at room temperature. (b) Response-recovery curve of $Ti_3C_2T_x$ activated with oxygen plasma to 10–800 ppm ethanol at room temperature. (c) Dynamic response-recovery curve of the $Ti_3C_2T_x$ activated with oxygen plasma to ethanol at 100 ppm. (d) Response of the raw $Ti_3C_2T_x$ and $Ti_3C_2T_x$ activated with oxygen plasma to different gases at 100 ppm. (e) Dynamic response-recovery curve of the $Ti_3C_2T_x$ activated with oxygen plasma to different gases at 100 ppm. (f) The stability of the $Ti_3C_2T_x$ activated at 500 °C with oxygen plasma at room temperature to 100 ppm ethanol.

Table 3
The gas sensing performance of $Ti_3C_2T_x$ activated with oxygen plasma at 500 °C toward ethanol compared with previous works.

Sensing material	Fabrication method	Operating temperature	Response	Refs.
V_2CT_x	Delamination	RT	1.75% @100 ppm	[44]
a-Fe_2O_3/MoS_2	Self-assembled	RT	88.9% @100 ppm	[45]
WS_2/WO_3	Self-assembled	RT	74.5%@50 ppm	[46]
TiO_2/WSe_2	LbL self-assembly	RT	211%@5 ppm	[47]
3-D MXene	Electronspinning self-assembly approach	RT	1.75%@10 ppm	[43]
$Ti_3C_2T_x$	Oxygen plasma activating	RT	22.47% @100 ppm	This work

conduction band of the activated $Ti_3C_2T_x$ to form chemisorbed oxygen ions. During the process, electron depletion layer will be generated on the samples' surfaces and it will cause an increase in sample resistance. Moreover, when putting the sample in VOCs gas (shown in Fig. 12 (b)), the VOCs gas will react with oxygen anions and the electrons trapped by the oxygen molecules will be released to the conduction band, which causes the depletion layer to narrow and increases the conductivity and reduces the resistance.

Compared with raw $Ti_3C_2T_x$; $Ti_3C_2T_x$ activated with oxygen microwave plasma has higher capacity of adsorbing oxygen on the materials surface and electronic transmission capacity. As displayed in Fig. 12 (c), oxygen plasma treatment process can provide a rich oxygen environment for MXene, in which the activated oxygen in the plasma can react with the hydroxyl groups of MXene to generate water, and compete with the fluorine functional group until F is gradually replaced. The amazing activation process increases the number of oxygen functional groups, which enriches the active site for oxygen adsorption of MXene (as shown in **Fig. 12 (a)**). The superior characteristics are conducive to the adsorption and desorption of gas molecules to improve the sensitive performance [48]. On the other hand, the increment of the oxygen functional group can improve the work function of the sample, thereby more electrons from conduction band will be captured and the efficiency

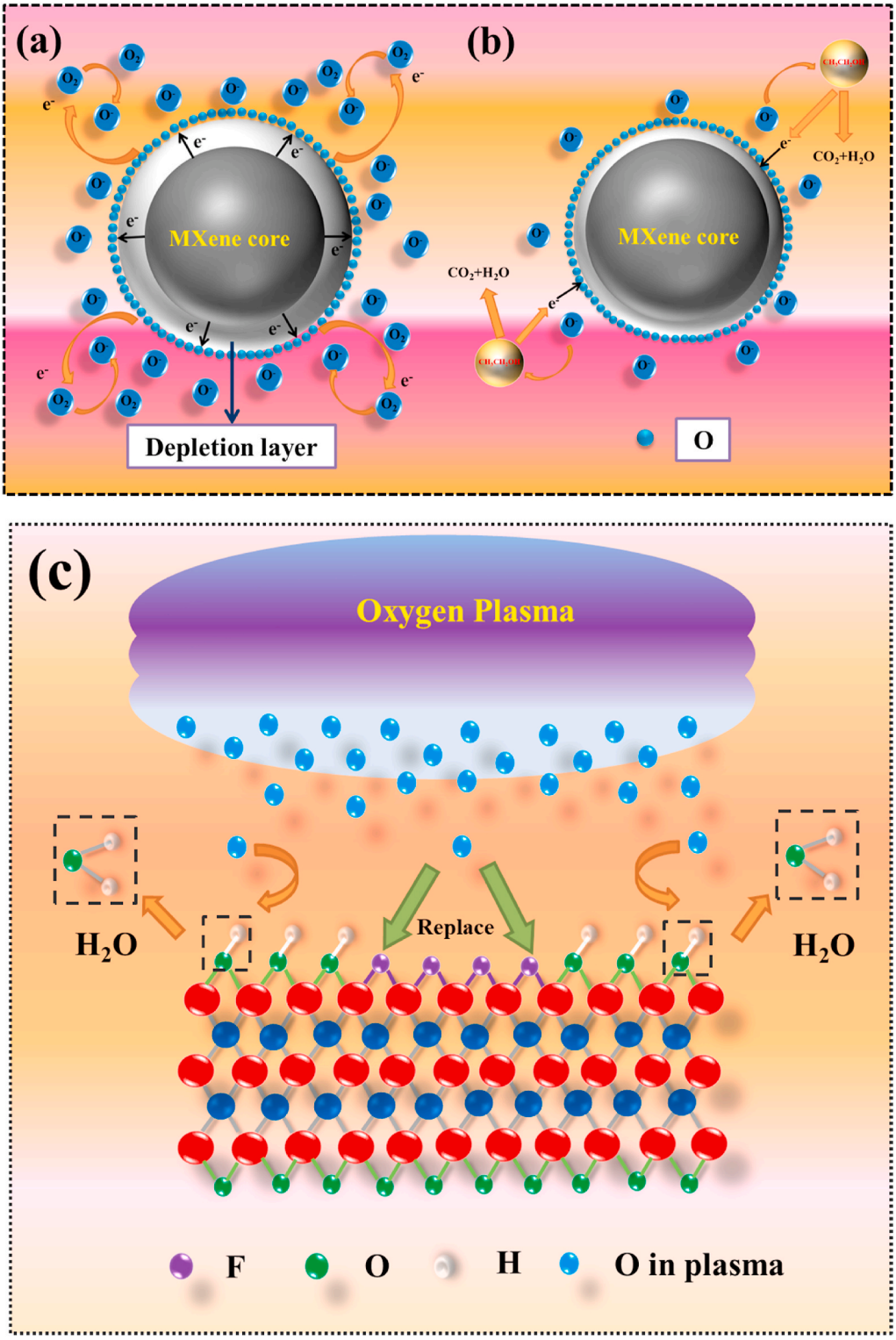

Fig. 12. Schematic diagram of the possible gas sensing mechanism of $Ti_3C_2T_x$ MXene.

of electron transmission will be improved to increase the gas sensing performance [49]. Therefore, $Ti_3C_2T_x$ possess great VOCs sensing performances after the oxygen plasma activation.

4. Conclusions

In summary, raw organ-like $Ti_3C_2T_x$ and activated $Ti_3C_2T_x$ sensors were prepared to study their gas sensing performances. The defects and increase of oxygen functional groups were observed and firmly characterized by various techniques. The gas-sensing properties of the raw $Ti_3C_2T_x$ and $Ti_3C_2T_x$ activated with oxygen microwave plasma were studied. Compared with raw $Ti_3C_2T_x$ sensors, the $Ti_3C_2T_x$ activated with oxygen microwave plasma shows more excellent gas sensing performance and it exhibits superior sensitive properties toward 100 ppm

ethanol at room temperature without any assistance. Such an improvement is attributed to the introduction of defects on the material and the increase of oxygen functional groups. This work has successfully developed a novel method to enhance the gas-sensing properties of $Ti_3C_2T_x$ MXene.

Declaration of competing interest

The authors declare that they have no known competing financial interests or personal relationships that could have appeared to influence the work reported in this paper.

Acknowledge

This research was funded by National Natural Science Foundation of China, No. 51864028; Yunnan Province Science and Technology Major Project for Materials Genetic Engineering of Rare and Precious Metal, No.202002AB080001; the Applied Basic Research Fund Project of Yunnan Province, No. 2018FD053 & No. 2018FA029; Yunnan Province Funds for Distinguished Young Scientists, No.; 2019FJ005 Yunnan Ten Thousand Talents Plan Young & Elite Talents Project, No. YNWRQNBJ-2018-311; The authors (Li Yang No. 201908530039, Ming Hou No. 201808740007) would like to acknowledge China Scholarship Council and Yunnan Ten Thousand Talents Plan of Study Abroad Project for the support of the Visiting Scholar's Program.

References

[1] X.H. Liu, T. Ma, N. Pinna, Two-dimensional nanostructured materials for gas sensing, Adv. Funct. Mater. 27 (2017) 1702168.
[2] X. Xing, Y. Yang, Z. Yan, Y. Hu, Y. Wang, CdO-Ag-ZnO nanocomposites with hierarchically porous structure for effective VOCs gas-sensing properties, Ceram. Int. 45 (2019) 4322–4334.
[3] W. Zhong, Q. Liu, Y. Wu, Y. Wang, X. Qing, M. Li, A nanofiber based artificial electronic skin with high pressure sensitivity and 3D conformability, Nanoscale 8 (2016) 12105–12112.
[4] Z. Jing, J. Zhan, Fabrication and gas-sensing properties of porous ZnO nanoplates, Adv. Mater. 20 (2010) 4547–4551.
[5] Y. Tang, B. Su, M. Liu, Superwettability strategy: 1D assembly of binary nanoparticles as gas sensors, Small 13 (2016) 1601087.
[6] K.S. Choi, S. Park, S.P. Chang, Enhanced ethanol sensing properties based on SnO_2 nanowires coated with Fe_2O_3 nanoparticles, Sens. Actuators, B 238 (2017) 871–879.
[7] A. Mirzaei, S.G. Leonardi, G. Neri, Detection of hazardous volatile organic compounds (VOCs) by metal oxide nanostructures-based gas sensors: a review, Ceram. Int. 42 (2016) 15119–15141.
[8] G. Shi, J. Liu, W. Zhao, Separation and purification and in vitro anti-proliferative activity of leukemia cell K562 of Galium aparine L. petroleum ether phase, Saudi Pharmaceut. J. 24 (2016) 241–244.
[9] M. John, Density measurement of ethanol blended fuels, Int. J. Mod. Phys. E: Conference Series 24 (2013) 1360009.
[10] ATSDR (Agency for Toxic Substances and Disease Registry), Toxicological Profile for Benzene, U.S. Public Health Service, U.S. Department of Health and Human Services, Atlanta, 1997.
[11] ATSDR (Agency for Toxic Substances and Disease Registry), Toxicological Profile for Toluene, U.S. Public Health Service, U.S. Department of Health and Human Services, Atlanta, 1994.
[12] IRIS, Integrated Risk Information System) on N-Hexane, U.S. EPA, National Centre for Environmental Assessment Office of Research and Development, Washington D. C., 1999.
[13] X. Wang, S. Li, L. Xie, X. Li, Z. Zhu, Low-temperature and highly sensitivity H_2S gas sensor based on ZnO/CuO composite derived from bimetal metal-organic frameworks, Ceram. Int. 46 (2020) 15858–15866.
[14] Y. Zhou, S. Chen, J. Sun, J. Liu, Y. Che, X. Liu, J. Zhang, D. Yang, Highly efficient gas sensor using a hollow SnO_2 microfiber for triethylamine detection, ACS Sens. 2 (2017) 897–902.
[15] X. Kou, C. Wang, M. Ding, Synthesis of Co-doped SnO_2 nanofibers and their enhanced gas-sensing properties, Sens. Actuators, B 236 (2016) 425–432.
[16] Z. Feng, Y. Ma, V. Natarajan, In-situ generation of highly dispersed Au nanoparticles on porous ZnO nanoplates via ion exchange from hydrozincite for VOCs gas sensing, Sens. Actuators, B 255 (2018) 884–890.
[17] Y. Chung, H. Park, E. Lee, S.H. Kim, D. Kim, Communication gas sensing behaviors of electrophoretically deposited nickel oxide films from morphologically tailored particles, Electrochem. Soc. 163 (2016) B624–B626.
[18] X. Tang, A.J. Du, L.Z. Kou, Gas sensing and capturing based on two-dimensional layered materials: overview from theoretical perspective, Wiley Interdiscip. Rev.: Comput. Mol. Sci. 8 (2018) 1361.
[19] B. Anasori, M.R. Lukatskaya, Y. Gogotsi, 2d metal carbides and nitrides (mxenes) for energy storage, Nat. Rev. Mater. 2 (2017) 16098.
[20] F. Shahzad, M. Alhabeb, C.B. Hatter, B. Anasori, S.M. Hong, C.M. Koo, Y. Gogotsi, Electromagnetic interference shielding with 2d transition metal carbides (mxenes), Sci. Asia 353 (2016) 1137–1140.
[21] M. Naguib, C. Jérémy, B. Dyatkin MXene, A promising transition metal carbide anode for lithium-ion batteries, Electrochem. Commun. 16 (2012) 61–64.
[22] Y.S.F. Han, L. Xie, C.C. Zhang, A MXene of type $Ti_3C_2T_x$ functionalized with copper nanoclusters for the fluorometric determination of glutathione, Microchim. Acta. 38 (2020) 187.
[23] F. Han, S. Luo, L. Xie, J. Zhu, W. Wei, Boosting the yield of MXene 2D sheets via a facile hydrothermal-assisted intercalation, ACS Appl. Mater. Interfaces 11 (2019) 8443–8452.
[24] S.J. Luo, L.Y. Xie, F. Han, W. Wei, Y. Huang, H. Zhang, Nanoscale parallel circuitry based on interpenetrating conductive assembly for flexible and high-power zinc ion battery, Adv. Funct. Mater. 29 (2019) 1901336.
[25] S.B. Sun, M.W. Wang, X.T. Chang, Y.C. Jiang, D.Z. Zhang, $W_{18}O_{49}/Ti_3C_2T_x$ Mxene nanocomposites for highly sensitive acetone gas sensor with low detection limit, Sens. Actuators, B 304 (2020) 127274.
[26] S.J. Kim, H.J. Koh, C.E. Ren, O. Kwon, K. Maleski, S.Y. Cho, B. Anasori, C.K. Kim, Y. K. Choi, J. Kim, Y. Gogotsi, H.T. Jung, Metallic $Ti_3C_2T_x$ MXene gas sensors with ultrahigh signal-to-noise ratio, ACS Nano 12 (2018) 986–993.
[27] E. Lee, A.V. Mohammadi, B.C. Prorok, Y.S. Yoon, M. Beidaghi, D.J. Kim, Room temperature gas sensing of two-dimensional titanium carbide (MXene), ACS Appl. Mater. Interfaces 9 (2017) 37184–37190.
[28] Z. Yang, A. Liu, C. Wang, F. Liu, J. He, S. Li, J. Wang, R. You, X. Yan, P. Sun, Y. Duan, G. Lu, Improvement of gas and humidity sensing properties of organ-like MXene by alkaline treatment, ACS Sens. 4 (2019) 1261–1269.
[29] I.I. Vlasov, A.S. Barnard, V.G. Ralchenko, Nanodiamond photo emitters based on strong narrow-band luminescence from silicon-vacancy defects, Adv. Mater. 21 (2009) 808–812.
[30] Y. Wu, H. Sugimura, Y. Inoue, Preparation of hard and ultra-water-repellent silicon oxide films by microwave plasma-enhanced CVD at low substrate temperatures, Thin Solid Films 435 (2003) 161–164.
[31] M. Hou, L. Yang, Q. Luo, Novel surface treatment strategy to improve the binding strength for diamond film on Ti substrate, Arabian J. Sci. Eng. 43 (2018) 263–270.
[32] Z. Raymundo, I. Rosa, N. Guadalupe, C. Víctor, J. Ku, B. Javier, A. Graciela, Surface modification of graphene nanoparticles with ethylene plasma in rotary plasma reactor for the preparation of GnP/HDPE nanocomposites, IEEE Trans. Plasma Sci. 7 (2018) 2402–2406.
[33] C.E. Shuck, M. Han, K. Maleski, Effect of Ti_3AlC_2 MAX phase on structure and properties of resultant $Ti_3C_2T_x$ MXene, ACS Appl. Nano Mater. 2 (2019) 3368–3376.
[34] M. Alhabeb, K. Maleski, B. Anasori, P. Lelyukh, L. Clark, S. Sin, Y. Gogotsi, Guidelines for synthesis and processing of 2D titanium carbide ($Ti_3C_2T_x$ MXene), Chem. Mater. 29 (2017) 7633−–7644.
[35] T. Yang, L. Du, C. Zhai, Ultrafast response and recovery trim ethylamine sensor based on α-Fe_2O_3, snowflake-like hierarchical architectures, J. Alloys Compd. 718 (2017) 396–404.
[36] H. Yu, T. Yang, Z. Wang, P-N heterostructural sensor with SnO-SnO_2, for fast NO_2, sensing response properties at room temperature, Sens. Actuators, B 258 (2018) 517–526.
[37] H. Yu, T. Yang, Facile synthesis cedar-like SnO_2 hierarchical micro-nanostructures with improved formaldehyde gas sensing characteristics, J. Alloys Compd. 724 (2017) 121–129.
[38] J.Y. Liu, M.J. Dai, T.S. Wang, P. Sun, X.S. Liang, G.Y. Lu, K. Shimanoe, N. Yamazoe, Enhanced gas sensing properties of SnO_2 hollow spheres decorated with CeO_2 nanoparticles heterostructure composite materials, ACS Appl. Mater. Interfaces 8 (2016) 6669–6677.
[39] S. Nundy, T. Eom, K. Song, J. Park, H. Lee, Hydrothermal synthesis of mesoporous ZnO microspheres as NOX gas sensor materials—calcination effects on microstructure and sensing performance, Ceram. Int. 46 (2020) 19354–19364.
[40] B. Zhang, G. Liu, M. Cheng, Y. Gao, L.J. Zhao, S. Li, F. Liu, X. Y, T. Zhang, P. S, G. Y. Lu, The preparation of reduced graphene oxide-encapsulated α-Fe_2O_3 hybrid and its outstanding NO_2 gas sensing properties at room temperature, Sens. Actuators, B 261 (2018) 252–263.
[41] Y.L. Wang, B. Zhang, J. Liu, Q.Y. Yang, X.B. Cui, Y. Gao, X.H. Chuai, F.M. Liu, P. Sun, X.S. Liang, Y.F. Sun, G.Y. Lu, Au-loaded mesoporous WO_3: preparation and n-butanol sensing performances, Sens. Actuators, B 236 (2016) 67–76.
[42] J. Liu, B. Zhang, Y. Xiao, Y. Gao, Q. Yang, Y. Wang, G.Y. Lu, Ultrasensitive and low detection limit of nitrogen dioxide gas sensor based on flower-like ZnO hierarchical nanostructure modified by reduced graphene oxide, Sens. Actuators, B 249 (2017) 715–724.
[43] W. Yuan, K. Yang, H. Peng, F. Li, F. Yin, A flexible VOCs sensor based on a 3D MXene framework with a high sensing performance, J. Mater. Chem. A. 6 (2018) 18116–18124.
[44] E.J. Lee, Y.S. Yoon, M.J. Beidaghi, D.J. Kim, Two-dimensional vanadium carbide MXene for gas sensors with ultrahigh sensitivity toward nonpolar gases, ACS Sens. 4 (2019) 1603–1611.
[45] D.Z. Zhang, X. Fan, A.J. Yang, X.Q. Zong, Hierarchical assembly of urchin-like alpha-iron oxide hollow microspheres and molybdenum disulphide nanosheets for ethanol gas sensing, J. Colloid Interface Sci. 523 (2018) 217–225.
[46] D.Z. Zhang, Y.H. Gao, J.F. Wu, X.X. Zhang, Tungsten trioxide nanoparticles decorated tungsten disulfide nanoheterojunction for highly sensitive ethanol gas sensing application, Appl. Surf. Sci. 503 (2020) 144063.

[47] W.J. Pan, Y. Zhang, D.Z. Zhang, Self-assembly fabrication of titanium dioxide nanospheres-decorated tungsten diselenide hexagonal nanosheets for ethanol gas sensing application, Appl. Surf. Sci. 527 (2020) 146781.
[48] C. Sergii, V.N. Mochalin, Environment-sensitive photoresponse of spontaneously partially oxidized Ti_3C_2 MXene thin films, ACS Nano 12 (2018) 6109–6116.
[49] J. Ran, G. Gao, F.T. Li, T.Y. Ma, A. DuS, Z. Qiao, Ti_3C_2 MXene co-catalyst on metal sulfide photo-absorbers for enhanced visible-light photocatalytic hydrogen production, Nat. Commun. 8 (2017) 13907.